



Synthesis, Spectroscopic, Computational Structure Analysis, Molecular Docking, *in vitro* Antibacterial and *in vivo* Antipyretic Investigations of Transition Metal(II) Complexes

P. YOGALAKSHMI^{1,*} and N. BANUMATHI²

¹Department of Chemistry, G. Venkataswamy Naidu College (Affiliated to Manonmaniam Sundaranar University), Kovilpatti-628502, India

²Department of Chemistry, Rani Anna Government College for Women (Affiliated to Manonmaniam Sundaranar University), Tirunelveli-627008, India

*Corresponding author: E-mail: s.dharu1996@yahoo.com

Received: 30 May 2023;

Accepted: 29 July 2023;

Published online: 2 December 2023;

AJC-21447

Unsymmetrical Schiff base hydrazone complexes of cobalt(II), nickel(II) and zinc(II) were synthesized from oxalic dihydrazide, salicylaldehyde and ethyl acetoacetate. The ligand and its metal(II) complexes were characterized by elemental analysis, UV-visible, FT-IR, molar conductivity. To determine the biological activity, *in vivo* antipyretic as well as *in vitro* antibacterial activities were conducted along with molecular docking simulation, HOMO-LUMO and MEP calculations. The findings from the experimental and molecular docking investigations demonstrated that the ligand and all the metal(II) complexes has an ability to interact with *E. coli* 24kDa domain protein (PDB: 1KZN). Furthermore, these interactions were accompanied by favourable docking score values, indicating potential therapeutic implications. The quantum parameters and geometric optimization of the ligand and complexes were performed using DFT simulations.

Keywords: Transition metal(II) complexes, Antibacterial analysis, Antipyretic analysis, Molecular docking.

INTRODUCTION

The characteristics of coordination compounds are greatly influenced by the choice of ligands. The addition of ligand frameworks containing electronegative atoms like nitrogen and oxygen improves the performance of coordination compounds [1]. The transition metal ions exhibit various optical, biological, chemical, electrical and magnetic properties with various Schiff base ligands [2-5]. It has been well-documented in the literature that the bioactivity of organic ligands can be influenced by metal coordination with Schiff base ligands [3-5]. In the biological field, there are more attempts to create novel transition metal complexes. Novel chemotherapeutic medicines must be created because many pathogenic germs have become resistant to already available antibacterial medications [6,7].

The chemistry and advantageous biological actions of the acyl hydrazone derivatives make them of great interest. For metabolism to function, there must be bioactivity due to the presence of different coordination centres that can form stable chelates with transition metal ions [8]. The synthesis of transition metal complexes with asymmetric Schiff base ligands is of increasing importance due to the asymmetrical nature

of the coordinating ligands surrounding the core metal ions systems.

There are numerous metal complexes of hydrazone derivatives that exhibit antialgae, antifungal, antibacterial and antitumor activity, according to reports [9-11]. Although the poly-functional ligand hydrazone can create more stable complexes with *d*-block elements, there are just a few articles that have been published that discuss unsymmetrical hydrazone ligands [12]. This might be because the oxalic dihydrazone ligand is poorly soluble in frequently used organic solvents but is so in highly polar solvents like DMSO and DMF and complexes with transition metal are prepared using the solid solution technique. According to a review of the literature, there have been relatively few studies on oxalic dihydrazide-based ligands that form unsymmetrical Schiff bases with salicylaldehyde and ethyl acetoacetate. The current work is focussed on these complexes and the metal complexes of the ligand are also discussed.

EXPERIMENTAL

All the chemicals and solvents were employed without further purification. From Sigma-Aldrich, diethyl oxalate, hydrazine hydrate, salicylaldehyde, ethyl acetoacetate, cobalt(II)

chloride, zinc(II) chloride and nickel(II) chloride were procured.

Physical measurements: A Perkin-Elmer FTIR spectrometer was used to capture the FT-IR spectra in the 4000-400 cm^{-1} region using KBr pellet method. The UV-1700 spectrometer, which has a frequency range of 200-600 nm, was utilized to capture the UV-visible spectrum. A 305 Systronic Conductivity Bridge was used to evaluate the complexes' molar conductance in DMSO solution.

Synthesis of ligand and metal complexes

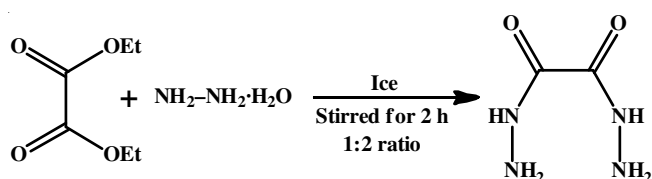
Preparation of oxalic dihydrazide: Diethyl oxalate and hydrazine monohydrate were combined in a 1:2 ratio while stirring continuously. The resulting compound was filtered off, washed repeatedly with water and ethanol and recrystallized from the distilled water-ethanol mixture to remove any excess hydrazine (m.p.: 240 °C) [13] (Scheme-I).

Synthesis of oxalic dihydrazone ligand (esodh-H): The ligand was synthesized by mixing a hot, diluted ethanolic solu-

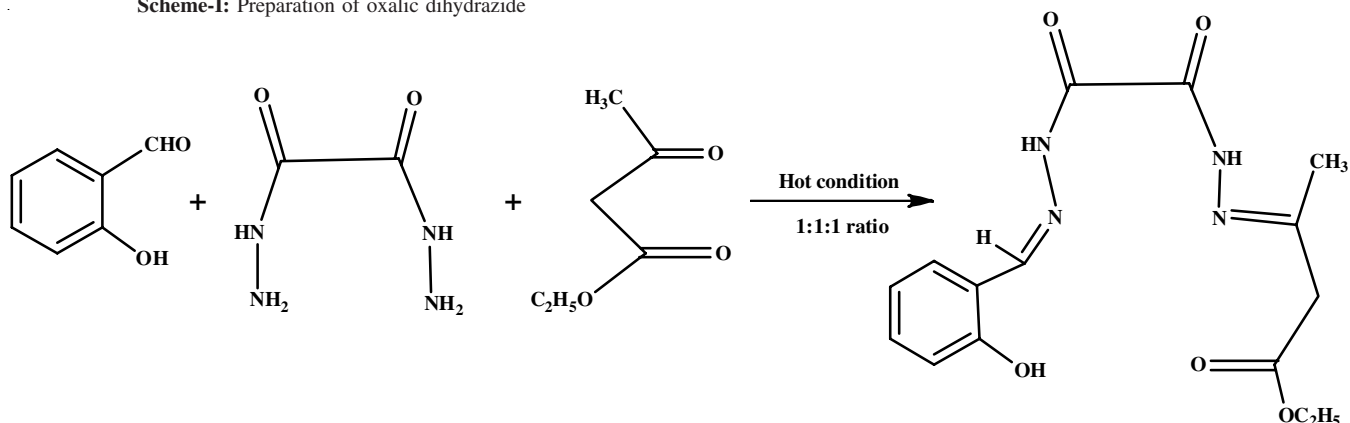
tion of oxalic dihydrazide with absolute ethanolic solution of salicylaldehyde and ethyl acetoacetate in a 1:1:1 molar ratio. The precipitate obtained was then filtered, washed with hot water to remove excess dihydrazide, whereas absolute ethanol was used to remove the excess aldehyde and diketone and dried *in vacuo* [14] (Scheme-II).

Synthesis of metal(II) complexes [M(esodh-H)]Cl: All the metal complexes were synthesized using the solid solution approach, which involved mixing a 1:1 mixture of metal salt (CoCl₂, NiCl₂ and ZnCl₂) and ligand in alcohol-water solvent (8:1) at room temperature while stirring. To complete the reaction, the mixture was refluxed for 5-6 h while being regularly shaken. The mixture was filtered and washed with an ethanol-water solution. The metal(II) complexes were purified by washing with ethanol and then dried on anhydrous CaCl₂ (Scheme-III).

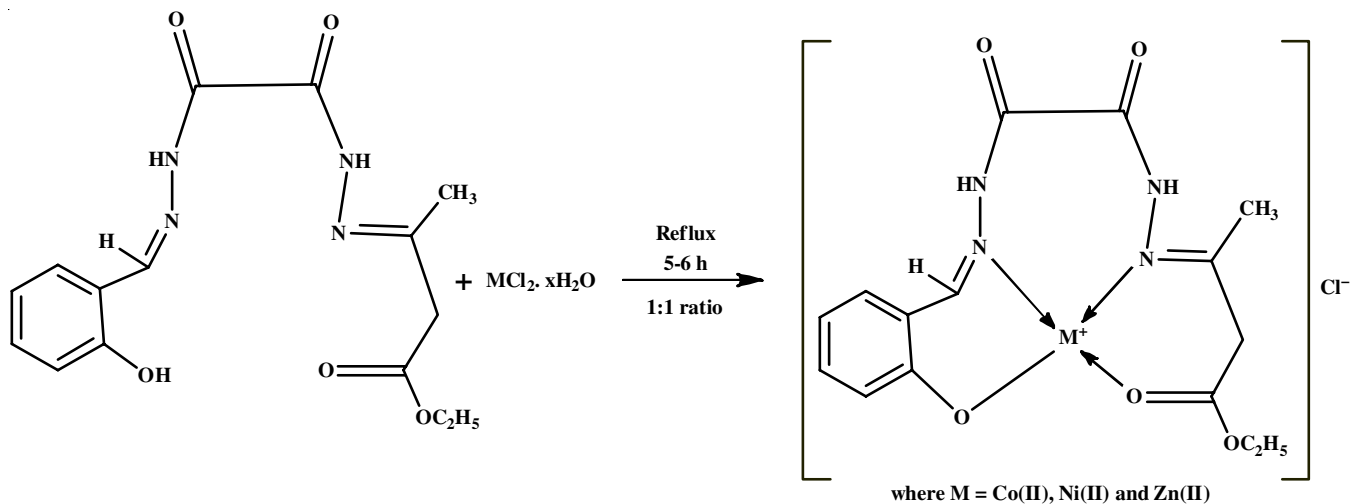
Computational quantum studies: The quantum computational geometry optimization of esodh-H ligand and its Ni(II), Co(II) and Zn(II) complexes were carried out using the ChemDraw structures as initial atomic coordinates with the Gaussian 09W program [15]. The ligand and metal(II) complexes structures were optimized to DFT ground state method using the default spin and GENIECP basis set mode. As additional inputs, Becke's 3-parameter hybrid exchange functional in combination with the Lee-Yang-Parr (LYP) correlation functional B3LYP/



Scheme-I: Preparation of oxalic dihydrazide



Scheme-II: Preparation of oxalic dihydrazone ligand (esodh-H)



Scheme-III: Preparation of the complexes [M(esodh-H)]Cl

6-31++G basis set for C, H, N and O atoms and for the metal atoms in the complexes Los Alamos National Laboratory 2 double zeta (LanL2DZ) basis set was applied [16]. The HOMO and LUMO molecular orbitals were visualized using the .chk file generated in Gaussian software. Using the generated total electron density cubes, molecular electrostatic potential (MESP) surfaces were drawn for the ligand and its metal(II) complexes.

Molecular docking analysis: To investigate the conformation modes of small molecules with the suitable target protein molecular docking method is popularly used in novel drug design processes. Ethyl (*E*)-3-(2-(2-((*E*)-2-hydroxy benzylidene)hydrazineyl)-2-oxoacetyl)hydrazineylidene)butanoate ligand and its metal(II) complexes were docked with the popular bacterial target crystal structure of *E. coli* 24kDa Domain protein. The 1KZN structure was obtained freely from RCSB PDB server [17]. Using the Discovery studio client 2016 package, the 1KZN macromolecule and DFT-optimized ligand structures were prepared for the molecular docking process. The active binding site grid sphere was selected using the coordination of the native ligand chlorobiocin present in 1KZN protein. The molecular docking investigations were carried out by the AutoDock Vina suit and the best docking pose having a higher docking score with various types of interactions was visualized using Discovery Studio client software [18-20].

Drug likeness properties: The molecular properties of the prepared compounds against the antibiotic streptomycin were studied using mol-inspiration online server to find whether the compounds obey Lipinski's rule and Veber's rule and found out their bioactivity [21].

In vitro antibacterial studies: The antibacterial effect of the synthesized ligand and metal(II) complexes against bacterial pathogens was investigated by the well-diffusion method. The cultures of *Staphylococcus aureus* and *Escherichia coli* were obtained and maintained in nutrient agar slant for bacteria at 37 °C. The bacterial strains were grown overnight in nutrient agar medium, on a rotary shaker (200 rpm) at 37 °C. The inoculum containing a microbial load of 1×10^5 CFU/mL was then applied to the respective agar plates. Wells of 6 mm diameter were punched aseptically with a sterile cork borer and further loaded with 100 µg/mL concentration of the compounds and

positive control streptomycin. The plates were then incubated for 24 h at 37 °C, for bacteria and the zone of inhibition (ZOI; mm) appearing around the wells was measured [22].

In vivo antipyretic studies

Antipyretic activity: Wistar rats of either sex weighing between 130 to 170 g was divided into groups of six animals each. Their initial rectal temperature was recorded by the insertion of a thermocouple to a depth of 2 cm into the rectum. The Brewer's yeast was injected subcutaneously in the back at a dose of 10 mL/kg and the yeast was suspended in 0.9% saline. The injection site was subjected to manual manipulation in order to disperse the suspension evenly beneath the skin. The room temperature was maintained between 22-24 °C. Immediately after the yeast injection the food was withdrawn and at 18 h post-challenge the rise in rectal temperature was recorded. Only animals with a body temperature of at least 38 °C were included in this test. The animals received the test compound or standard drug by oral administration and their rectal temperature was recorded at 30, 60, 120 and 180 min thereafter. The maximum reduction in average rectal temperature was calculated and the results were compared with the standard drug like paracetamol [23].

RESULTS AND DISCUSSION

The analytical data (Table-1) demonstrated that the unsymmetrical condensation of ethyl acetoacetate and salicylaldehyde with oxalic dihydrazide yields the ligand esodh-H. When the ligand combines with metal(II) chloride, the phenolic proton on the ligand deprotonates, forming 1:1 complexes with a typical composition $[M(\text{esodh-H})]Cl$. The synthesized ligand and its metal(II) complexes are soluble in DMF and DMSO, but insoluble in chloroform, benzene and diethyl ether.

The infrared, electronic spectral and molar conductance data for the ligand and its metal(II) complexes are shown in Table-2. In order to ascertain the ability of the coordination sites involved in chelation, the infrared spectra of the metal(II) complexes were compared to that of the uncoordinated ligand. The unsymmetrical Schiff base ligand esodh-H exhibits bands at 3499 and 3193 cm^{-1} which is attributed due to the phenolic

TABLE-1
PHYSICAL CHARACTERIZATION AND ANALYTICAL DATA OF THE COMPOUNDS

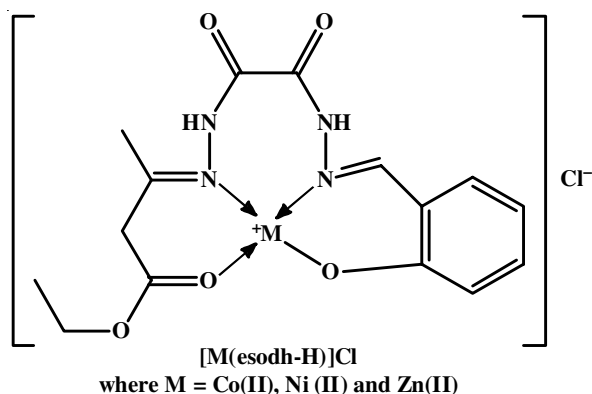
Compound	Yield (%)	m.p./ decomp.* (°C)	Colour	Elemental analysis (%): Found (calcd.)			m.w.
				C	H	N	
(esodh-H)	80	> 200	White	56.11 (56.09)	4.56 (4.43)	19.53 (19.46)	334.33
[Co(esodh-H)Cl]	75	> 200	Yellow	58.25 (58.12)	4.68 (4.61)	17.25 (17.10)	427.71
[Ni(esodh-H)Cl]	80	> 200	Light yellow	58.35 (58.15)	4.63 (4.61)	17.42 (17.11)	427.47
[Zn(esodh-H)Cl]	85	> 200	Cream	56.91 (56.49)	4.80 (4.75)	17.09 (17.01)	434.18

TABLE-2
INFRARED, ELECTRONIC SPECTRAL AND MOLAR CONDUCTANCE DATA FOR THE LIGAND AND COMPLEXES

Compound	$\nu(\text{OH})$	$\nu(\text{NH})$	$\nu(\text{COOR})$	$\nu(\text{C=O})$	$\nu(\text{C=N})$	Amide I	Amide II	$\nu(\text{C-O})$	$\nu(\text{N-N})$	$\lambda_m (\text{Ohm}^{-1} \text{cm}^2 \text{mol}^{-1})$	$\lambda_{\text{max}} (\text{Å})$
(esodh-H)	3499	3193	1720	1665	1624	1530	1356	—	976	—	290, 320, 340
[Co(esodh-H)Cl]	—	3193	1788	1669	1605	1527	1355	1263	993	58	292, 327, 345, 436
[Ni(esodh-H)Cl]	—	3198	1730	1662	1601	1531	1356	1258	1033	60	292, 327, 343
[Zn(esodh-H)Cl]	—	3198	1736	1663	1601	1532	1356	1258	1033	65	292, 327, 343

(O-H) and (N-H) present because of two amide >NH groups, respectively. The amide (N-H) band in metal complexes either occurs at the same frequency as in the parent ligand or is only slightly shifted, which indicates that the N-H group is not involved in the bonding. Moreover, it can be seen from the band at 3499 cm^{-1} that phenolic (O-H) did not establish a hydrogen bond. The deprotonation of the phenolic proton (O-H) during complexation is indicated by the absence of the (O-H) band in all the metal complexes. A new band at $1263\text{--}1258\text{ cm}^{-1}$, which is attributed to phenolic (C-O) in the metal complexes, further supports this. Due to the presence of two amide >C=O groups of dihydrazide and an ester group of ethyl acetoacetate with carbonyl stretching vibrations, the ligand exhibits two >C=O bands at 1720 cm^{-1} and 1665 cm^{-1} , respectively [24].

The carbonyl stretching vibration of the ester group can be attributed to intense bands in the spectra of the Schiff base at 1720 cm^{-1} . This band increased in frequency at $1788\text{--}1730\text{ cm}^{-1}$ during complexation, indicating coordination *via* the ester carbonyl group [25]. In dihydrazide, a band due to >C=O group slightly shifted indicated that two amide >C=O groups are not involved in the bonding process. The presence of the keto group in the solid state is confirmed by the ligand's appearance of the >C=O and -N-H bands *i.e.* in unenolized form. The amide-II (1530 cm^{-1}) and amide-III (1356 cm^{-1}) bands for the unenolized ligand are either same or slightly shifted in the metal(II) complexes, indicating the coordination of ethyl acetoacetate to the metal ion through the ester carbonyl group with the metal ion. The (C=N) band observed at 1624 cm^{-1} in ligand confirmed the interaction of dihydrazide with the aldehyde and keto group of ethyl acetoacetate as the band is shifted to a lower frequency by $19\text{--}23\text{ cm}^{-1}$ in its metal(II) complexes, implying that the coordination occurs through the two azomethine groups. In its complexes, the weak band of ligand caused by (N-N) moves to a higher frequency by $17\text{--}57\text{ cm}^{-1}$, indicating that one of the nitrogen atoms in N-N coordinates with the metal ions [26]. As a result, it can be inferred from the IR spectra that the ligand behaves as a monobasic tetradentate ligand coupled to metal ion *via* phenolic oxygen of salicylaldehyde, the carbonyl oxygen of ethyl acetoacetate and nitrogen of azomethine groups of both compounds. The metal complex may be ascribed to the following broad structure (Scheme-IV) as a result of the aforementioned finding.



Scheme-IV: Representative structures of the metal complexes [M(esodh-H)]Cl

Electronic spectral studies: At 300 K, the electronic absorption spectra of the Schiff base complexes of Ni(II), Co(II) and Zn(II) were measured. The electronic spectra can be utilized to determine the structure of metal(II) complexes in the absence of X-ray diffraction studies because the quantity and location of spectral bands reveal details about the geometry of the metal complexes. Cobalt(II) complex electronic spectra exhibit a band at 436 cm^{-1} that is associated with $d \rightarrow \pi^*$ MLCT (combination of ${}^2B_{1g} \rightarrow {}^2A_{1g}$ and ${}^1B_{1g} \rightarrow {}^2A_{1g}$) [27-29].

Nickel(II) complex electronic spectra were found below 600 cm^{-1} . The square planar structure of the nickel(II) complex is consistent with the absence of any electronic transition at longer wavelengths. As a result, it may be easily separated from octahedral and tetrahedral complexes. The results are particularly significant because they were strongly influenced by the molecule's shape. Since the complex's shape is similar to that of a square planar complex, the smaller the value, the shorter the wavelength of the band corresponding to the transition [30-32].

Molar conductivity: At ambient temperature, the molar conductivity of the complexes measured using DMSO as solvent at 10^{-3} M show that the complexes behave as 1:1 electrolytes, with conductivity values in the range of $55\text{ to }65\ \Omega^{-1}\text{ mol}^{-1}\text{ cm}^2$. As a result, the complexes are tentatively assigned as [M(esodh-H)]Cl, where M is Co^{2+} , Ni^{2+} or Zn^{2+} [33].

Quantum computational analysis: To better understand the synthesized ligand and its metal(II) complexes structures, using the Gaussian 09 package, quantum computational geometry optimization were performed in the gaseous phase. The optimized ground state structures of free ligand esodh-H (Fig. 1) and its Co(II), Ni(II) and zinc metal complexes are represented in Fig. 2. The DFT optimized bond distances for free ligand esodh-H are N1-N2 = 1.380 \AA , N3-N4 = 1.387 \AA , C7-N1 = 1.302 \AA , C10-N4 = 1.296 \AA , C8-O1 = 1.245 \AA , C9-O2 = 1.246 \AA , C12-O3 = 1.231 and O5-C12-O3 bond angle is 118.6° . The DFT optimized bond distances for [Ni(esodh-H)]Cl are Ni-O3 = 2.192 \AA , Ni-O4 = 1.9471 \AA , Ni-N1 = 2.046 \AA , Ni-N4 = 2.0315 \AA , for [Co(esodh-H)]Cl are Co-O3 = 2.008 \AA , Co-O4 = 1.864 \AA , Co-N1 = 1.906 \AA , Co-N4 = 1.923 \AA and for [Zn(esodh-H)]Cl are Zn-O3 = 2.113 \AA , Zn-O4 = 1.940 \AA , Zn-N1 = 2.064 \AA , Zn-N4 = 2.052 \AA . The >C=N- bond distances for [Ni(esodh-H)]Cl are C7-N1 = 1.323 \AA , C10-N4 = 1.464 \AA , for [Co(esodh-H)]Cl are C7-N1 = 1.328 \AA , C10-N4 = 1.313 \AA .

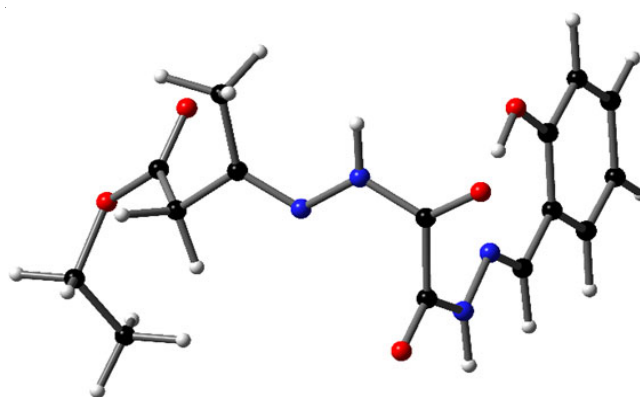


Fig. 1. DFT optimized structure of free ligand esodh-H

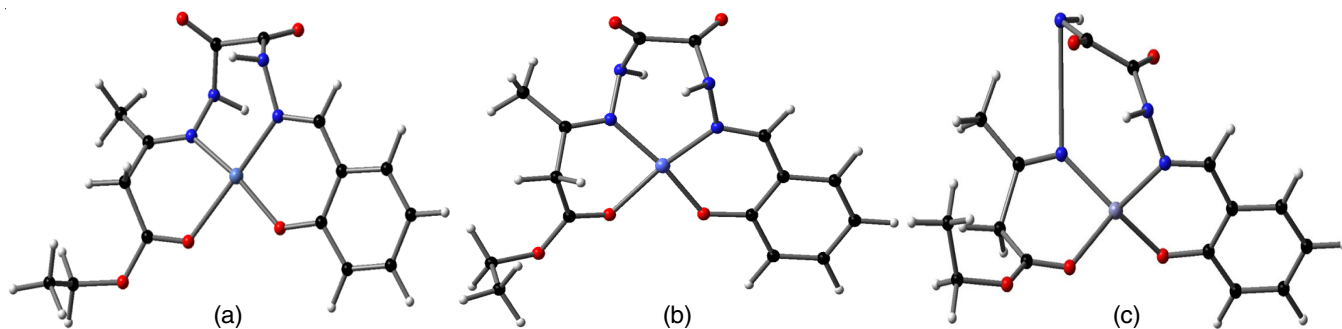


Fig. 2. DFT optimized structure of (a) Ni(II), (b) Co(II) and (c) Zn(II) complexes of esodh-H

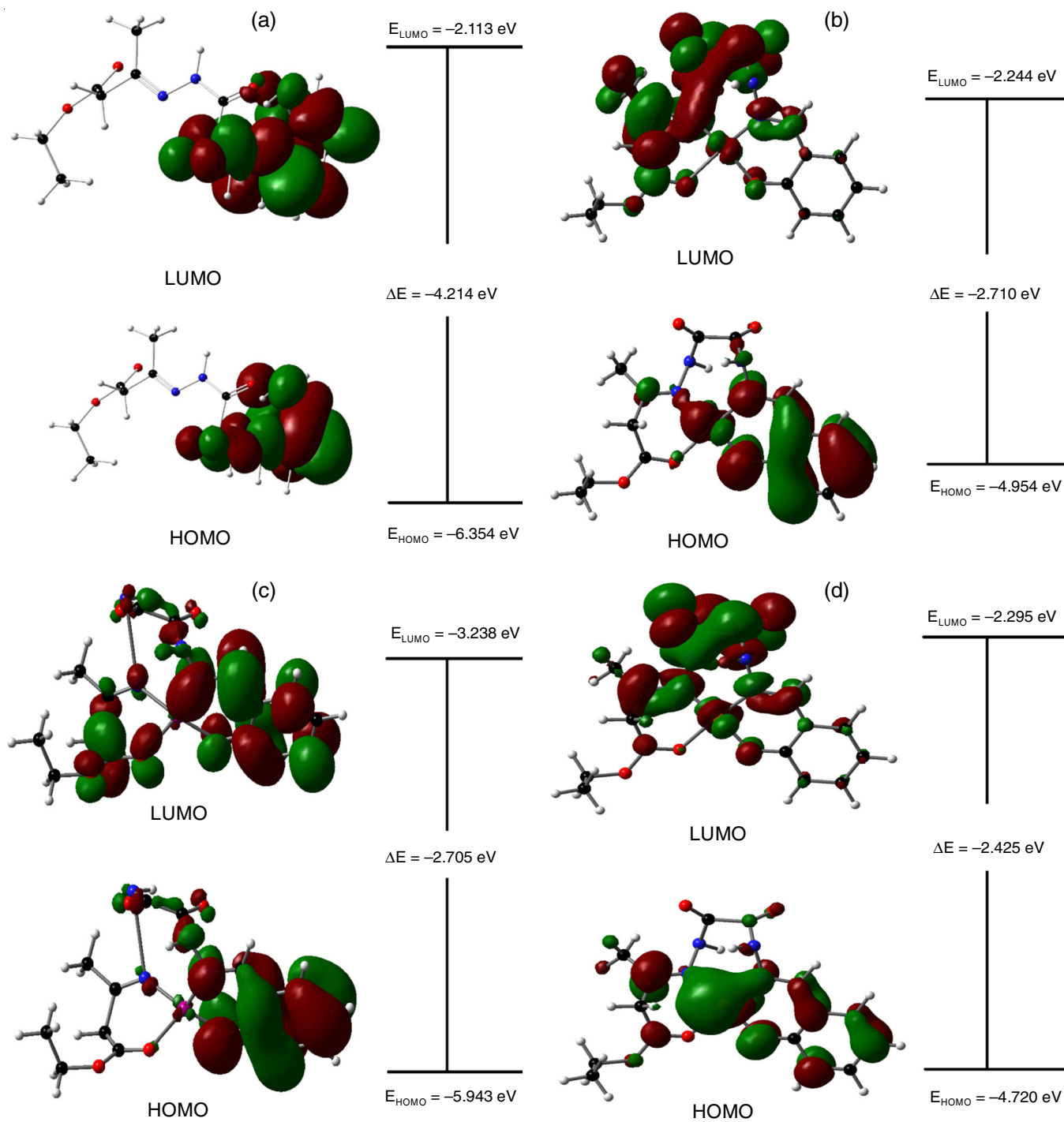


Fig. 3. Molecular orbital energy gap of (a) esodh-H, (b) [Ni(esodh-H)]Cl, (c) [Zn(esodh-H)]Cl and (d) [Co(esodh-H)]Cl

Å and for [Zn(esodh-H)]Cl are C7-N1 = 1.314 Å, C10-N4 = 1.266 Å. The >C=O bond distances for [Ni(esodh-H)]Cl are C8-O1 = 1.234 Å, C9-O2 = 1.237 Å, C12-O3 = 1.237 Å, for [Co(esodh-H)]Cl are C8-O1 = 1.232 Å, C9-O2 = 1.235 Å, C12-O3 = 1.245 Å and for [Zn(esodh-H)]Cl are C8-O1 = 1.234 Å, C9-O2 = 1.237 Å, C12-O3 = 1.256 Å.

The O5-C12-O3 bond angles at 117.9°, 117.5° and 116.33° were assigned for Ni, Co and Zn metal complexes of esodh-H, respectively. The bond angles of complexes N1-Ni-N4 (102.4°), O3-Ni-O4 (88.6°), N1-Ni-O4 (88.9°), N4-Ni-O3 (82.4°), N1-Co-N4 (100.5°), O3-Co-O4 (84.1°), N1-Co-O4 (91.2°), N4-Ni-O3 (95.6°), N1-Zn-N4 (105.1°), O3-Zn-O4 (109.6°), N1-Zn-O4 (91.2°), N4-Zn-O3 (87.5°) are in correlation with the reports of analogous structures [34-36]. In Ni, Co and Zn metal complexes, the linked six-membered heterometallacycles are square planar as represented in Fig. 2.

Using the Frontier molecular orbitals (FMO) theory, we can precisely predict the interactive nature of drug like molecules with target receptors. The excitation energy of molecules could be computed by finding the energy difference between the unoccupied molecular orbital (LUMO) and the highest occupied molecular orbital (HOMO) [37]. The significant frontier molecular orbitals (HOMO and LUMO) were drawn for the ligand and its metal(II) complexes using the DFT/B3LYP/6-31++G and LanL2DZ (for metal atoms) levels and shown in Fig. 3 with respective energy values. The molecular orbital energy gap value of ligand, [Co(esodh-H)]Cl, [Ni(esodh-H)]Cl and [Zn(esodh-H)]Cl were -4.214 eV, -2.425 eV, -2.710 eV and -2.705 eV, respectively as represented. The lower energy gap value of our metal complexes indicates the quick charge transfer nature between the two molecular orbitals which refers to the increased bioactivity of the synthesized complexes.

The molecular electrostatic map (MEP) is extensively used to recognize both the structural and electronic properties of druglike compounds [38]. The MEP exhibits electrophilic (red

region) and nucleophilic (blue region) attack regions that help to validate the drug interaction with target proteins. The MEP of the metal(II) complexes was computed using DFT/B3LYP/6-31++G and LanL2DZ (for metal atoms) method and shown in Fig. 4. From the MEP diagram, the negatively charged potential (electrophilic) regions were observed around both oxygen atoms linked with metal atoms, C8=O1 and C9=O2 atoms, which clearly infers the reactive sites of the complexes.

Molecular docking studies: To analyze the interaction ability of the esodh-H based metal(II) complexes and drug clorobiocin was docked into the active binding site of DNA gyrase bacterial protein PDB ID-KZN. The top binding conformation was chosen based on the lowest binding energy. The binding energy values were -9.53 kcal/mol, -9.27 kcal/mol, -9.46 kcal/mol, -9.83 kcal/mol and -9.65 kcal/mol, for ligand esodh-H, [Ni(esodh-H)]Cl, [Co(esodh-H)]Cl, [Zn(esodh-H)]Cl and clorobiocin, respectively.

Ligand [esodh-H]-1KZN docked complex was stabilized with three conventional hydrogen bonds, four carbon-hydrogen bond interactions, one π -cation bond and four hydrophobic bonds with binding energy -9.53 kcal/mol. The amino acid GLY77 bound with the oxygen atom O2 and N2-H atom through a bifurcated hydrogen bond. Similarly, the hydrogen atom attached with N2 atom of [esodh-H] ligand interacted with amino acid GLU50 through a N-H...O type hydrogen bonds at a distance of 3.042 Å. In addition, one π -cation bond with residue ARG76 and hydrophobic bonds with residues VAL43, ALA47, VAL71 and PRO79 were also observed (Fig. 5).

The [Ni(esodh-H)]Cl-1KZN docked complex revealed one conventional hydrogen bond interaction, three carbon-hydrogen bond interactions, one π - σ (sigma) bond and eleven hydrophobic interactions with binding energy -9.27 kcal/mol. The 3D and 2D representation of [Ni(esodh-H)]Cl-1KZN docked complex is shown in Fig. 6. The amino acid ASN46 interacted with the oxygen atom O3 attached with Ni²⁺ of [Ni(esodh-H)]Cl

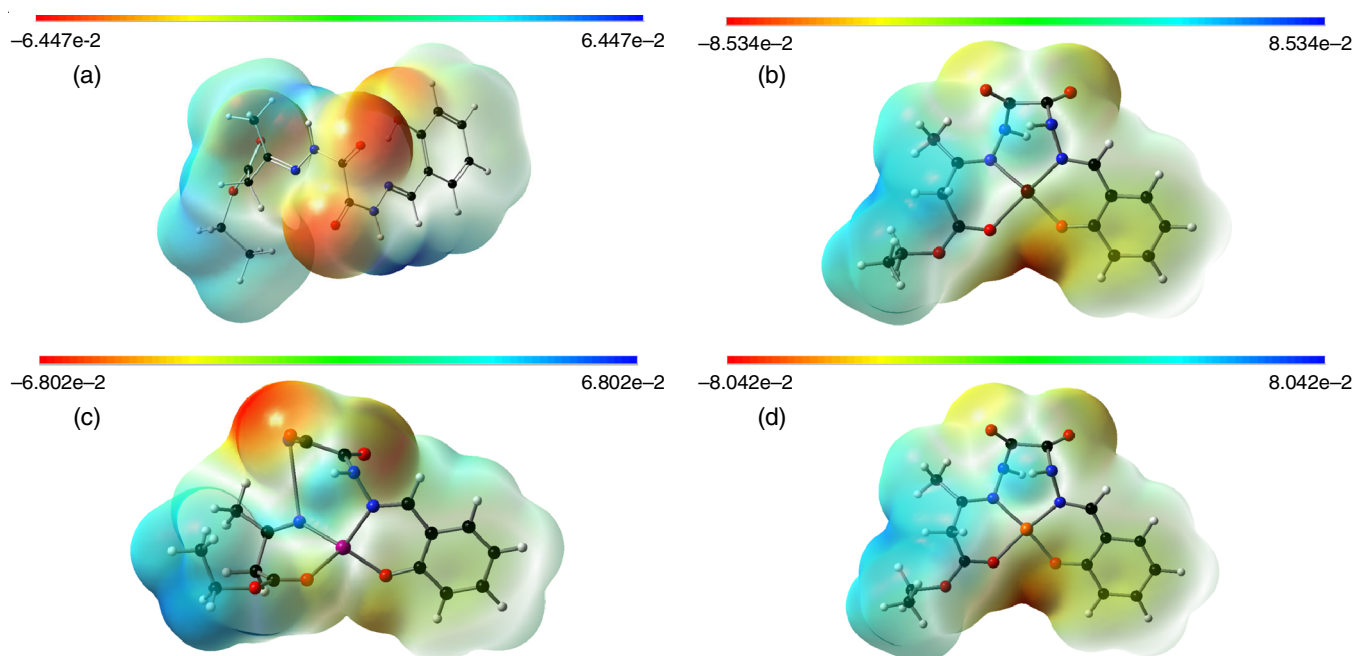


Fig. 4. Molecular electrostatic map of (a) ligand esodh-H, (b) [Ni(esodh-H)]Cl, (c) [Zn(esodh-H)]Cl and (d) [Co(esodh-H)]Cl

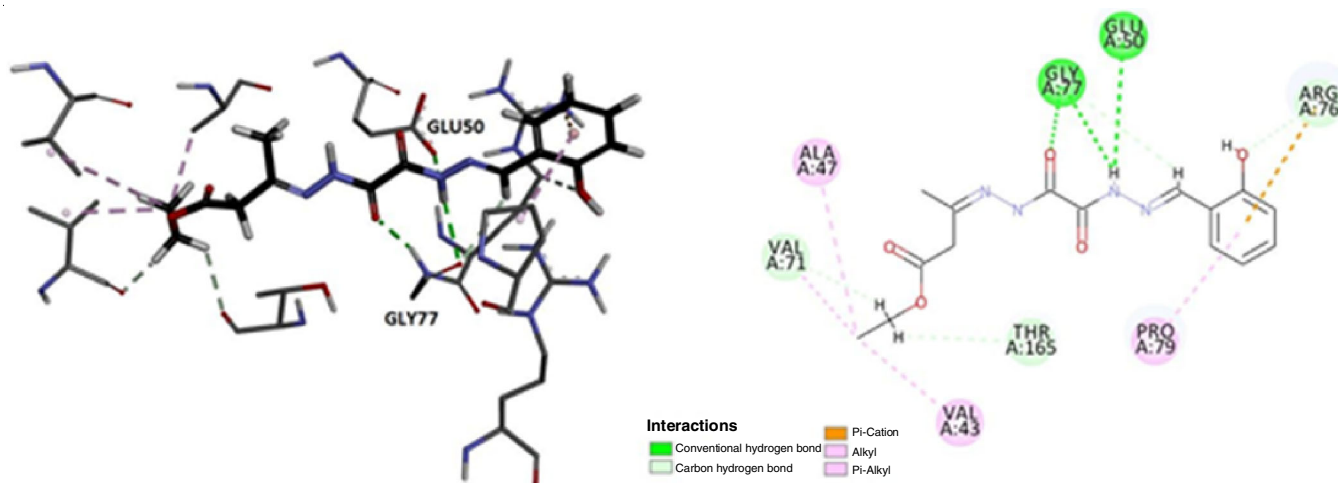


Fig. 5. Docking interactions of [esodh-H] with amino acids of DNA gyrase 1KZN bacterial protein

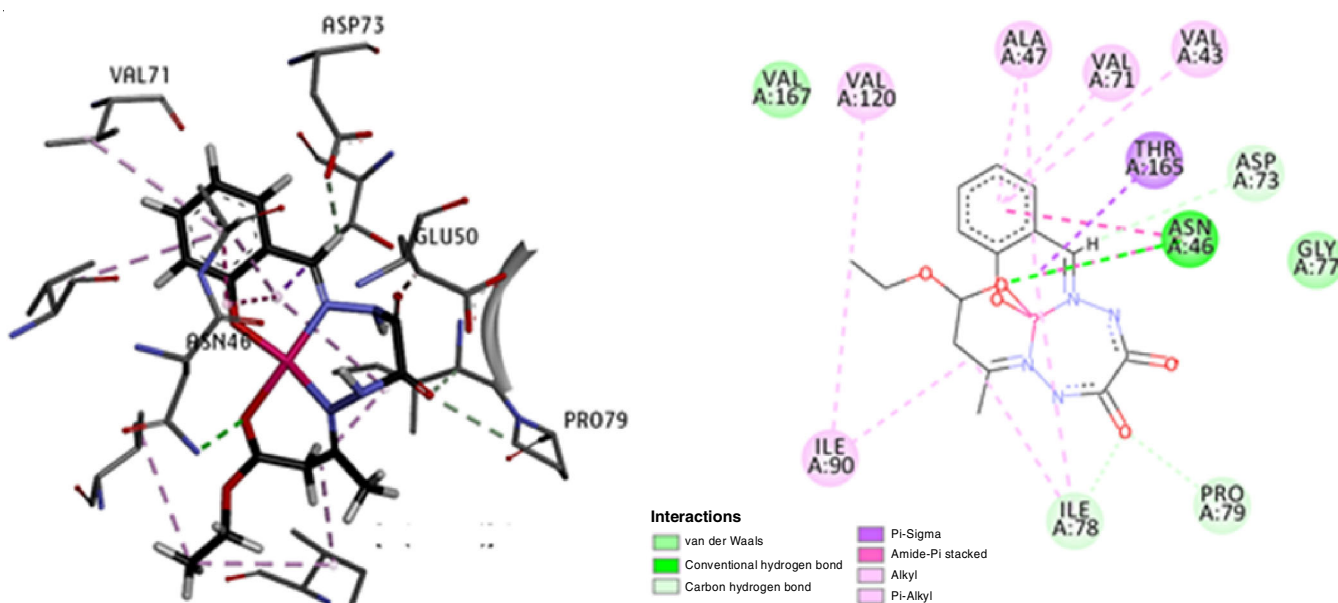


Fig. 6. Docking interactions of [Ni(esodh-H)]Cl with amino acids of DNA gyrase 1KZN bacterial protein

through a hydrogen bond ASN46:ND2...O2 at a distance of 2.750 Å. Likewise, the oxygen atom of [Ni(esodh-H)]Cl ligand bound with amino acids ILE78 and PRO79 through a bifurcated C-H...O type hydrogen bonds at a distance of 3.318 Å and 3.761 Å, respectively. It was also observed that one π - σ bond between residue THR165 and six-membered heterometallacycle (Ni/O2/C1,C6-C7) moiety. Additionally, the residues VAL43, ASN46, ALA47, VAL71, ILE78, ILE90 and VAL120 involved in different hydrophobic bonds with ligand [Ni(esodh-H)]Cl.

In [Co(esodh-H)]Cl-1KZN docked complex, two conventional hydrogen bond interactions, one carbon hydrogen bond interactions, one π - σ (sigma) bond and seven hydrophobic interactions were observed with binding energy -9.46 kcal/mol. The 3D and 2D illustration of [Co(esodh-H)]Cl-1KZN complex is shown in Fig. 7. The residue ASN46 bound with nitrogen atom N3 and oxygen atom O3 atom of ligand [Co(esodh-H)]Cl through N3-H...ASN46 and ASN46:ND2...O3 hydrogen bonds at a distance of 2.132Å and 2.486 Å, respectively. The oxygen atom OD1 atom of residue ASP73 interacted with [Co(esodh-

H)]Cl ligand through a carbon hydrogen bond (C7-H...OD1: ASP73) at a distance of 2.456 Å. One π - σ bond between residue THR165 and six-membered ring (C1-C6). Also, the active site residues ASN46, ALA47, VAL71, ILE90, VAL120 and VAL167 were bound by [Co(esodh-H)]Cl through several hydrophobic interactions as shown in Fig. 7.

The [Zn(esodh-H)]Cl-1KZN docked complex exceptionally stabilized with five conventional hydrogen bonds, one carbon-hydrogen bond, one pi-sigma bond and four hydrophobic bonds with the highest binding energy -9.83 kcal/mol. The 3D and 2D diagram of [Zn(esodh-H)]Cl-1KZN interactions is shown in Fig. 8. The active site amino acids GLU50, ASP73 (bifurcated), ARG76 and GLY77 were well connected with ligand [Zn(esodh-H)]Cl through five hydrogen bonds at a distance ranging 2.270-2.756 Å. In addition residue ASP73 formed a C7-H...OD1 bond with [Zn(esodh-H)]Cl ligand at a distance of 2.154 Å. One pi-sigma bond was identified between residue VAL167 and benzene moiety (C1-C6). Further, the amino acids ASN46, VAL71, ILE78 and PRO79 were connected

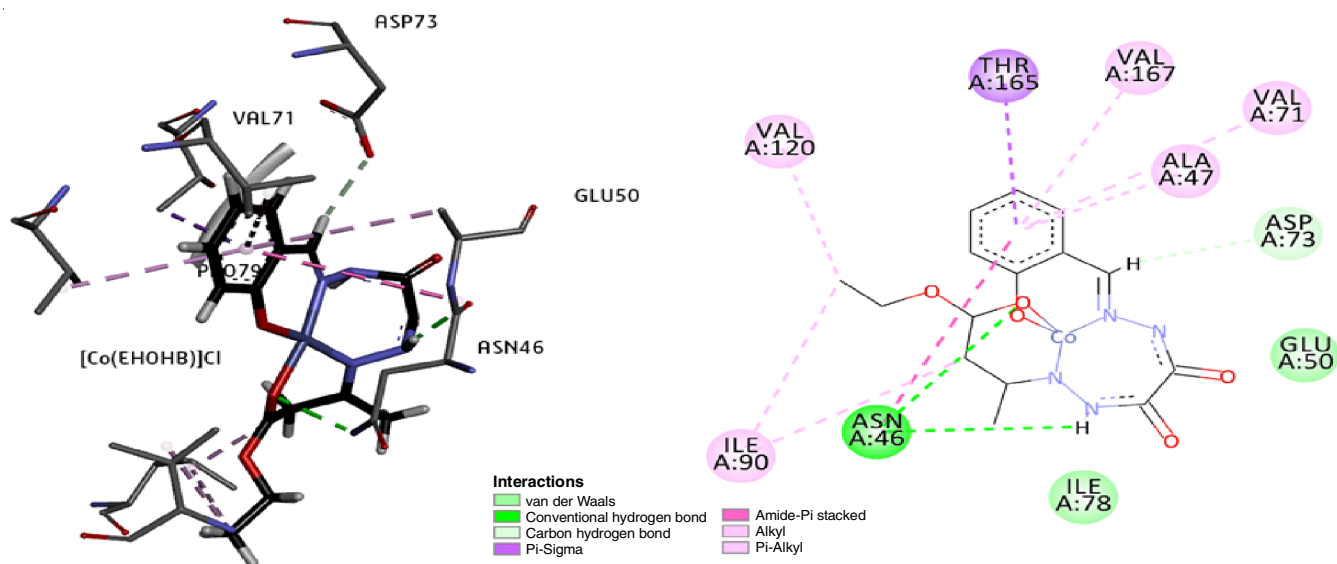


Fig. 7. Docking interactions of [Co(esodh-H)]Cl with amino acids of DNA gyrase 1KZN bacterial protein

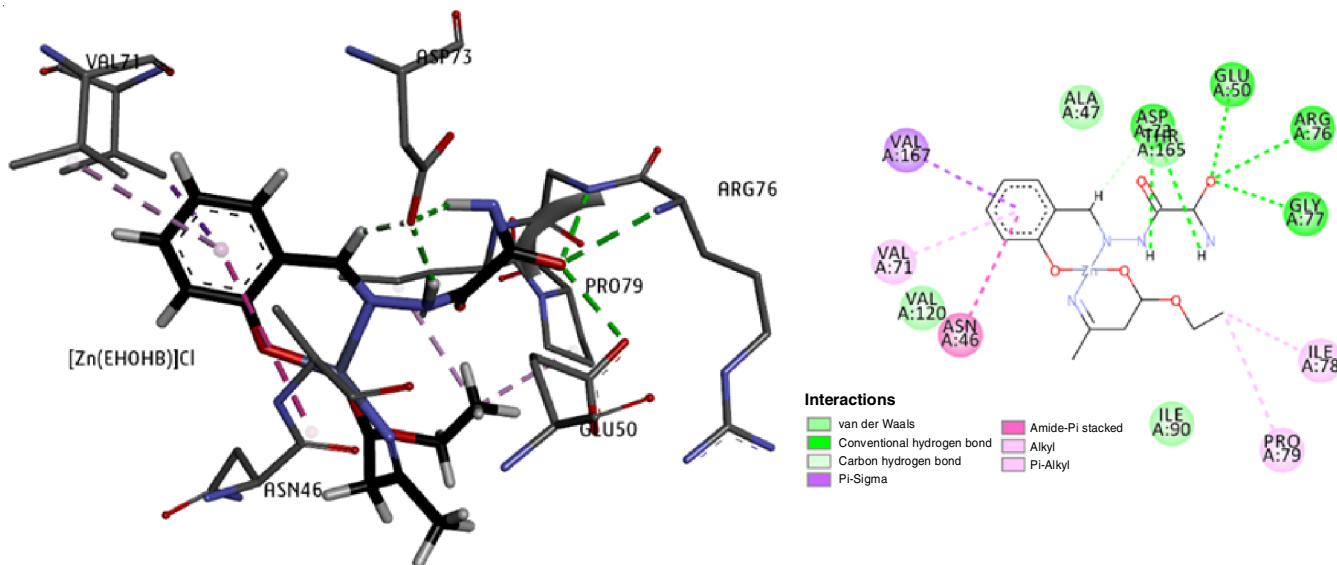


Fig. 8. Docking interactions of [Zn(esodh-H)]Cl with amino acids of DNA gyrase 1KZN bacterial protein

with [Zn(esodh-H)]Cl through hydrophobic bonds as shown in Fig. 8.

To correlate and validate the molecular docking analysis, the native ligand and popular bacterial DNA gyrase inhibitor clorobiocin was redocked with 1KZN protein. The clorobiocin-1KZN complex (binding energy -9.65 kcal/mol) revealed strong hydrogen bonds and hydrophobic interactions with binding site residues ASN46, ARG76, ILE78, ILE90, HIS95, ALA96, VAL120 and GLY117 as depicted in Fig. 9. The clorobiocin redocking investigation validates the binding nature of [Ni(esodh-H)]Cl, [Co(esodh-H)]Cl and [Zn(esodh-H)]Cl with bacterial DNA gyrase 1KZN by a similar type of interactions with active site residues. The findings indicate a strong correlation between the docking results and the reports from similar docking investigations [39].

Drug likeness properties: In present work, the molecular weight of the synthesized ligand was found to be less than

500 and satisfies the Lipinski rule and Veber's rule and the metal(II) complexes derived from this have a good drug-like background when compared with the reference drug streptomycin (Table-3), the synthesized compounds have drug-like properties. There is no violation of the Lipinski's rule by the synthesized compounds while the reference drug streptomycin has three violations, the new compounds also obey the Veber's rule and streptomycin has one violation as per the Veber rule.

In vitro antibacterial analysis: The *Bacillus subtilis*, *Staphylococcus aureus*, *Escherichia coli* and *Candida albicans* bacterial pathogens were used to analyze the antibacterial ability of the ligand and its metal(II) complexes. The zone of inhibition measured (mm) against bacterial pathogen strains is listed in Table-4. The zone of inhibition values of zinc complex with bacterial pathogens are closer to the control drug and correlates with the docking results except for *Candida albicans*. This confirms the higher inhibition ability of zinc(II) complex

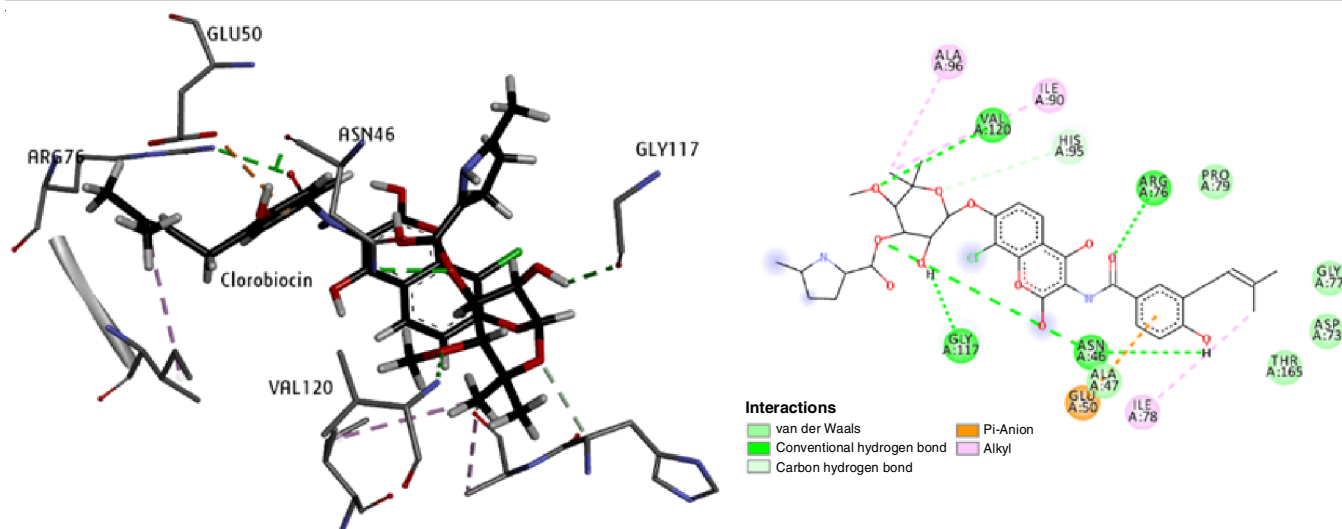


Fig. 9. Docking interactions of Clorobiocin with amino acids of DNA gyrase 1KZN bacterial protein

[Zn(esodh-H)]Cl. Similarly, the nickel complex exhibited the second highest zone of inhibition values with *Staphylococcus aureus* and *Escherichia coli*, whereas [Co(esodh-H)]Cl complex revealed a better inhibition value with *Candida albicans* next to the control drug.

In vitro Antipyretic analysis: The present study results showed that the sample drugs [Co(esodh-H)]Cl, [Ni(esodh-H)]Cl, [Zn(esodh-H)]Cl and (esodh-H) possess significant antipyretic activity (Table-5). The [Co(esodh-H)]Cl at 200 mg/kg dose exhibited significant antipyretic activity ($p < 0.05$) at 0 min, 1 h, 2 h and 4 h compared to the standard drug (paracetamol). At a higher dose (400 mg/kg), the antipyretic activity was higher and more significant ($p < 0.001$). While [Ni(esodh-H)]Cl at 200 mg/kg dose exhibited moderately significant antipyretic activity ($p < 0.01$) at 0, 1, 2 and 4 h compared to the standard drug. However, at a higher dose (400 mg/kg), the antipyretic activity was statistically significant, compared to the standard drug.

However, [Zn(esodh-H)]Cl at 200mg/kg dose did not show a significant antipyretic activity compared to the standard drug. But at the higher dose (400 mg/kg), the sample showed highly significant antipyretic activity ($p < 0.001$) compared to the standard drug. In case of ligand (esodh-H), at 200 mg/kg dose exhibit moderately significant antipyretic activity ($p < 0.01$) but at a higher dose (400 mg/kg), the antipyretic activity was increased and become highly significant ($p < 0.001$) compared to the standard drug.

Conclusion

In present study, the synthesis, characterization, DFT studies, molecular docking studies, *in vitro* antimicrobial activity and *in vivo* antipyretic activity of cobalt(II), nickel(II) and zinc(II) unsymmetrical Schiff base complexes derived by the condensation of oxalic dihydrazide with ethyl acetoacetate and salicylaldehyde are reported. The colour change of the ligand during

TABLE-3
DRUG LIKENESS PROPERTIES-LIPINSKI'S RULE AND VEBER'S RULE

Property	(esodh-H)	[Co(esodh-H)]Cl	[Ni(esodh-H)]Cl	[Zn(esodh-H)]Cl	Streptomycin
MW (< 500 daltons)	334.33	427.71	427.47	434.18	581.58
miLog P (< 5)	0.92	-2.85	-2.85	-2.52	-5.35
nON (HBA < 10)	9	9	9	9	19
nOHNH (HBD < 5)	3	2	2	2	16
n violations (Lipinski rule)	0	0	0	0	3
nrotb (<= 10)	8	9	9	9	9
TPSA (< 140 Å ²)	129.46	118.46	118.46	118.46	336.45
n violations (Veber rule)	0	0	0	0	1

TABLE-4
ZONE OF INHIBITION (mm) OBSERVED AGAINST BACTERIAL PATHOGENS BY SCHIFF BASE LIGAND AND METAL COMPLEXES

Compound	<i>Bacillus subtilis</i>	<i>Staphylococcus aureus</i>	<i>Escherichia coli</i>	<i>Candida albicans</i>
esodh-H	11 ± 0.23	12 ± 0.12	15 ± 0.28	13 ± 0.36
[Ni(esodh-H)]Cl	13 ± 0.42	17 ± 0.18	16 ± 0.75	12 ± 0.42
[Co(esodh-H)]Cl	12 ± 0.15	13 ± 0.59	15 ± 0.24	17 ± 0.14
[Zn(esodh-H)]Cl	16 ± 0.31	20 ± 0.19	19 ± 0.32	15 ± 0.05
Streptomycin (Positive)	19 ± 0.25	21 ± 0.09	22 ± 0.07	22 ± 0.27

Data are means (n = 3) ± standard deviation of three replicates; Zone of inhibition (diameter in mm) at a concentration of 100 µg.

TABLE-5
ANTIPYRETIC ACTIVITY DATA

Drug & dose	Before administration	0 min	1 h	2 h	4 h
Control (normal saline) 5 mL/kg (p.o)	38.1 ± 0.21	41.2 ± 1.23	41.3 ± 1.31	41.6 ± 1.43	41.4 ± 1.39
Standard paracetamol 100 mg/kg p.o.	38.3 ± 0.12***	41.7 ± 1.34*	40.5 ± 0.96**	39.1 ± 0.41**	37.8 ± 0.14***
[Co(esodh-H)]Cl 200 mg/kg p.o.	38.1 ± 0.11***	42.1 ± 1.43*	41.3 ± 1.12*	40.1 ± 0.87**	39.4 ± 0.32**
[Co(esodh-H)]Cl 400 mg/kg p.o.	38.2 ± 0.18***	41.9 ± 1.31***	40.5 ± 1.02***	39.6 ± 0.21	38.5 ± 0.17**
[Ni(esodh-H)]Cl 200 mg/kg p.o.	37.8 ± 0.08**	42.1 ± 1.65**	40.9 ± 1.22***	40.1 ± 0.82**	39.1 ± 0.47**
[Ni(esodh-H)]Cl 400 mg/kg p.o.	37.9 ± 0.17**	42.3 ± 1.57**	39.8 ± 0.91	38.9 ± 0.43	38.1 ± 0.13***
[Zn(esodh-H)]Cl 200 mg/kg p.o.	37.8 ± 0.09**	41.6 ± 1.37	39.3 ± 0.65	38.7 ± 0.38	38.0 ± 0.19***
[Zn(esodh-H)]Cl 400 mg/kg p.o.	38.0 ± 0.11***	41.8 ± 1.41***	39.7 ± 0.72	39.1 ± 0.31***	38.4 ± 0.22***
(esodh-H) 200 mg/kg p.o.	37.5 ± 0.07	41.4 ± 1.27	40.6 ± 0.69***	40.1 ± 0.27**	39.5 ± 0.21*
(esodh-H) 400 mg/kg p.o.	37.8 ± 0.13	41.7 ± 1.34***	40.1 ± 0.33	39.4 ± 0.24***	38.2 ± 0.14***

Values are mean ± SEM; n = 6 in each group; Group-II was compared with Group-I. Remaining groups were compared with Group-II. The values of mean were altered significantly *** $p < 0.001$ highly significant; ** $p < 0.01$ moderately significant; * $p < 0.05$ significant.

the complexation process can be considered as further evidence for the formation of required complexes. The empirical formula of Schiff base ligand and its metal(II) complexes were in agreement with the elemental analysis, FT-IR, UV and molar conductance data. The unsymmetrical Schiff base ligand and their complexes are stable at room temperature and soluble in water, DMF and DMSO solvents and the ligand effectively coordinated with metal ions *via* the two azomethine nitrogen atoms and two oxygen atoms of ethyl acetoacetate and salicylaldehyde respectively. The antibacterial activities of the Schiff base ligand and its metal(II) complexes revealed that only zinc(II) complex showed good antibacterial activity against both Gram-positive and Gram-negative bacterial strains as compared to the Schiff base ligand and closer to the control drug, streptomycin. The molecular docking studies also revealed that the cobalt(II) complex showed excellent binding to the receptor responsible for the antibacterial effect when compared to the clorobiocin drug. The qualitative and quantitative information on the reactive area were obtained using MEP studies. The drug-likeness studies confirmed that all the compounds have pharmaceutical properties based on Lipinski's rule and Veber's rule. Except for the unsymmetrical Schiff base ligand, all the complexes have a smaller HOMO-LUMO energy gap and cobalt(II) complex has the least energy gap of -2.425 eV. *In vivo* studies on the antipyretic activity confirmed that except for Ni(II) complex, other compounds show highly significant antipyretic activity when compared to the standard drug, paracetamol.

CONFLICT OF INTEREST

The authors declare that there is no conflict of interests regarding the publication of this article.

REFERENCES

- M.A. Malik, O.A. Dar, P. Gull, M.Y. Wani and A.A. Hashmi, *Med. Chem. Commun.*, **9**, 409 (2018); <https://doi.org/10.1039/C7MD00526A>
- A. Soroceanu and A. Bargan, *Crystals*, **12**, 1436 (2022); <https://doi.org/10.3390/cryst12101436>
- M.S. More, P.G. Joshi, Y.K. Mishra and P.K. Khanna, *Mater. Today Chem.*, **14**, 100195 (2019); <https://doi.org/10.1016/j.mtchem.2019.100195>
- A. Kanwal, B. Parveen, R. Ashraf, N. Haider and K.G. Ali, *J. Coord. Chem.*, **75**, 2533 (2022); <https://doi.org/10.1080/00958972.2022.2138364>
- A.M. Abu-Dief and I.M.A. Mohamed, *Beni-Suef Univ. J. Basic Appl. Sci.*, **4**, 119 (2015); <https://doi.org/10.1016/j.bjbas.2015.05.004>
- R. Khojasteh and S.J. Matin, *Russ. J. Appl. Chem.*, **88**, 921 (2015); <https://doi.org/10.1134/S107042721506004X>
- S. Hou, J. Li, X. Huang, X. Wang, L. Ma, W. Shen, F. Kang and Z.-H. Huang, *Appl. Sci.*, **7**, 852 (2017); <https://doi.org/10.3390/app7080852>
- N. Goswami and D.M. Eichhorn, *Inorg. Chim. Acta*, **303**, 271 (2000); [https://doi.org/10.1016/S0020-1693\(00\)00047-5](https://doi.org/10.1016/S0020-1693(00)00047-5)
- V.P. Singh, S. Singh and D.P. Singh *J. Enzyme Inhib. Med. Chem.*, **27**, 319 (2012); <https://doi.org/10.3109/14756366.2011.588228>
- V.P. Singh, A. Katiyar and S. Singh, *Biometals*, **21**, 491 (2008); <https://doi.org/10.1007/s10534-008-9136-9>
- V.P. Singh and P. Gupta, *J. Coord. Chem.*, **61**, 3922 (2008); <https://doi.org/10.1080/00958970802160974>
- J.-L. Wang, Y.-Q. Zhao and B.-S. Yang, *Inorg. Chim. Acta*, **409**, 484 (2014); <https://doi.org/10.1016/j.ica.2013.09.001>
- A.M. Hassan, A.H. Ahmed, H.A. Gumaa, B.H. Mohamed and A.M. Eraky, *J. Chem. Pharm. Res.*, **7**, 91 (2015).
- K.K. Narang and R.A. Lal, *Curr. Sci.*, **46**, 401 (1977).
- M. J. Frisch, G. W. Trucks, H. B. Schlegel, G. E. Scuseria, M. A. Robb, J. R. Cheeseman, G. Scalmani, V. Barone, G. A. Petersson, H. Nakatsuji, X. Li, M. Caricato, A. Marenich, J. Bloino, B. G. Janesko, R. Gomperts, B. Mennucci, H. P. Hratchian, J. V. Ortiz, A. F. Izmaylov, J. L. Sonnenberg, D. Williams-Young, F. Ding, F. Lipparini, F. Egidi, J. Goings, B. Peng, A. Petrone, T. Henderson, D. Ranasinghe, V. G. Zakrzewski, J. Gao, N. Rega, G. Zheng, W. Liang, M. Hada, M. Ehara, K. Toyota, R. Fukuda, J. Hasegawa, M. Ishida, T. Nakajima, Y. Honda, O. Kitao, H. Nakai, T. Vreven, K. Throssell, J. A. Montgomery, Jr., J. E. Peralta, F. Ogliaro, M. Bearpark, J. J. Heyd, E. Brothers, K. N. Kudin, V. N. Staroverov, T. Keith, R. Kobayashi, J. Normand, K. Raghavachari, A. Rendell, J. C. Burant, S. S. Iyengar, J. Tomasi, M. Cossi, J. M. Millam, M. Klene, C. Adamo, R. Cammi, J. W. Ochterski, R. L. Martin, K. Morokuma, O. Farkas, J. B. Foresman, and D. J. Fox, Gaussian, Inc., Wallingford CT, Gaussian 09, Revision A.02 (2016).
- Y. Yang, M.N. Weaver and K.M. Merz Jr., *J. Phys. Chem. A*, **113**, 9843 (2009); <https://doi.org/10.1021/jp807643p>
- F.T.F. Tsai, O.M.P. Singh, T. Skarzynski, A.J. Wonacott, S. Weston, A. Tucker, R.A. Pauptit, A.L. Breeze, J.P. Poyser, R. O'Brien, J.E. Ladbury and D.B. Wigley, *Proteins*, **28**, 41 (1997); [https://doi.org/10.1002/\(SICI\)1097-0134\(199705\)28:1<41::AID-PROT4>3.0.CO;2-M](https://doi.org/10.1002/(SICI)1097-0134(199705)28:1<41::AID-PROT4>3.0.CO;2-M)
- O. Trott and A.J. Olson, *J. Comput. Chem.*, **31**, 455 (2010); <https://doi.org/10.1002/jcc.21334>
- R. Huey, G.M. Morris and S. Forli, Using AutoDock 4 and AutoDock Vina with AutoDockTools: A Tutorial. The Scripps Research Institute Molecular Graphics Laboratory (2012).

20. D.S. Biovia, Discovery Studio Visualizer, San Diego, CA, USA, p. 936 (2017).
21. Molinspiration Cheminformatics free web services; <https://www.molinspiration.com> (Accessed on 22 March 2023).
22. M. Balouiri, M. Sadiki and S.K. Ibsouda, *J. Pharm. Anal.*, **6**, 71 (2016); <https://doi.org/10.1016/j.jpaha.2015.11.005>
23. C.A. Winter, E.A. Riskey and G.W. Nuss, *Exp. Biol. Med.*, **111**, 544 (1962); <https://doi.org/10.3181/00379727-111-27849>
24. V.P. Singh, S. Singh, D.P. Singh, K. Tiwari and M. Mishra, *J. Mol. Struct.*, **1058**, 71 (2014); <https://doi.org/10.1016/j.molstruc.2013.10.046>
25. N. Sathya, G. Raja, N.P. Priya and C. Jayabalakrishnan, *Appl. Organometal. Chem.*, **24**, 366 (2010); <https://doi.org/10.1002/aoc.1621>
26. V.P. Singh and P. Gupta, *J. Coord. Chem.*, **61**, 3922 (2008); <https://doi.org/10.1080/00958970802160974>
27. B. Oritz and S.M. Park, *Bull. Korean Chem. Soc.*, **21**, 405 (2000); <https://doi.org/10.5012/bkcs.2000.21.4.405>
28. M. Shakir, O.S.M. Nasman, A.K. Mohamed and S.P. Varkey, *Polyhedron*, **15**, 1283 (1996); [https://doi.org/10.1016/0277-5387\(95\)00379-7](https://doi.org/10.1016/0277-5387(95)00379-7)
29. L.S. Chen and S.C. Cummings, *Inorg. Chem.*, **17**, 2358 (1978); <https://doi.org/10.1021/ic50187a005>
30. R. Atkins, G. Brewer and E. Kokot, G.M. Mockler and E. Sinn, *Inorg. Chem.*, **24**, 127 (1985); <https://doi.org/10.1021/ic00196a003>
31. M. Kwiatkowski, E. Kwiatkowski, A. Olechnowicz, D.M. Ho and E. Deutsch, *J. Chem. Soc., Dalton Trans.*, 2497 (1990); <https://doi.org/10.1039/DT9900002497>
32. A.B.P. Lever, *Inorganic Electronic Spectroscopy*, New York: Elsevier edn. 2 (1984).
33. W.J. Geary, *Coord. Chem. Rev.*, **7**, 122 (1971); [https://doi.org/10.1016/S0010-8545\(00\)80009-0](https://doi.org/10.1016/S0010-8545(00)80009-0)
34. V.P. Singh, S. Singh, D.P. Singh, K. Tiwari and M. Mishra, *J. Mol. Struct.*, **1058**, 71 (2014); <https://doi.org/10.1016/j.molstruc.2013.10.046>
35. A. Amiri, M. Amirnasr, S. Meghdadi, K. Mereiter, V. Ghodsi and A. Gholami, *Inorg. Chim. Acta*, **362**, 3934 (2009); <https://doi.org/10.1016/j.ica.2009.05.020>
36. V.P. Singh, *Spectrochim. Acta A Mol. Biomol. Spectrosc.*, **71**, 17 (2008); <https://doi.org/10.1016/j.saa.2007.11.004>
37. D.H. Pereira, F.A.L. Porta, R.T. Santiago, D.R. Garcia and T.C. Ramalho, *Revista Virtual de Quimica*, **8**, 425 (2016); <https://doi.org/10.5935/1984-6835.20160032>
38. D. Shin and Y. Jung, *Phys. Chem. Chem. Phys.*, **24**, 25740 (2022); <https://doi.org/10.1039/D2CP03244A>
39. S. Murugavel, S. Deepa, C. Ravikumar, R. Ranganathan and P. Alagusundaram, *J. Mol. Struct.*, **1222**, 128961 (2020); <https://doi.org/10.1016/j.molstruc.2020.128961>